Arp2/3 complex inhibition radically alters lamellipodial actin architecture, suspended cell shape, and the cell spreading process

John H. Henson[a,b], Mesrob Yeterian[a], Richard M. Weeks[a], Angela E. Medrano[a], Briana L. Brown[a], Heather L. Geist[a], Mollyann D. Pais[a], Rudolf Oldenbourg[b], and Charles B. Shuster[b,c]
[a]Department of Biology, Dickinson College, Carlisle, PA 17013; [b]Marine Biological Laboratory, Woods Hole, MA 02543; [c]Department of Biology, New Mexico State University, Las Cruces, NM 88003

ABSTRACT **Recent studies have investigated the dendritic actin cytoskeleton of the cell edge's lamellipodial (LP) region by experimentally decreasing the activity of the actin filament nucleator and branch former, the Arp2/3 complex. Here we extend these studies via pharmacological inhibition of the Arp2/3 complex in sea urchin coelomocytes, cells that possess an unusually broad LP region and display correspondingly exaggerated centripetal flow. Using light and electron microscopy, we demonstrate that Arp2/3 complex inhibition via the drug CK666 dramatically altered LP actin architecture, slowed centripetal flow, drove a lamellipodial-to-filopodial shape change in suspended cells, and induced a novel actin structural organization during cell spreading. A general feature of the CK666 phenotype in coelomocytes was transverse actin arcs, and arc generation was arrested by a formin inhibitor. We also demonstrate that CK666 treatment produces actin arcs in other cells with broad LP regions, namely fish keratocytes and *Drosophila* S2 cells. We hypothesize that the actin arcs made visible by Arp2/3 complex inhibition in coelomocytes may represent an exaggerated manifestation of the elongate mother filaments that could possibly serve as the scaffold for the production of the dendritic actin network.**

Monitoring Editor
Laurent Blanchoin
CEA Grenoble

Received: Jul 30, 2014
Revised: Nov 26, 2014
Accepted: Dec 30, 2014

INTRODUCTION

A significant amount of research over the past decade has undergirded the development of the dendritic nucleation model of how actin filaments polymerize and are structured at the leading edge of cells (Pollard and Borisy, 2003; Chhabra and Higgs, 2007; Le Clainche and Carlier, 2008; Ridley, 2011; Svitkina, 2013). At the core of this model is the actin filament-nucleating Arp2/3 complex, a series of seven proteins that orchestrates the generation of the dendritic arrays of branched actin filaments characteristic of the lamellipodium (LP)—the outermost portion of the cell cortex, which undergoes rapid protrusion, retraction, and retrograde/centripetal flow (Goley and Welch, 2006; Pollard, 2007). A number of studies have focused on inhibition of the Arp2/3 complex as a means of determining the exact role that it plays and how other actin polymerization nucleators/facilitators might contribute to the LP. Approaches have included using small interfering RNA (Rogers *et al.*, 2003; Steffan *et al.*, 2006; Korobova and Svitkina, 2008; Nicholson-Dystra and Higgs, 2008) and genetic methods (Steffan *et al.*, 2006; Suraneni *et al.*, 2012; Wu *et al.*, 2012) to knock down or delete an Arp2/3 complex component. Alternatively, the function of the Arp2/3 complex has been interfered with via sequestration due to the presence of an Arp2/3 complex–binding WCA domain from one of the WASP family proteins (Machesky and Insall, 1998; Strasser *et al.*, 2004; Koestler *et al.*, 2013)—the nucleation-promoting factor proteins that serve as a bridge between signal transduction pathways and activation of the Arp2/3 complex. In addition, there have been pharmacological approaches ranging from the relatively nonspecific, employing the drug 2,3-butanedione monoxime (BDM; Yarrow *et al.*, 2003; Henson *et al.*, 2009), to the highly specific CK drugs expressly designed for Arp2/3 complex inhibition (Nolen *et al.*, 2009; Wu *et al.*, 2012; Yang *et al.*, 2012; Koestler *et al.*, 2013;

This article was published online ahead of print in MBoC in Press (http://www.molbiolcell.org/cgi/doi/10.1091/mbc.E14-07-1244) on January 7, 2015.

Address correspondence to: John Henson (henson@dickinson.edu).

Abbreviations used: BDM, 2,3-butanedione monoxime; CCM, coelomocyte culture medium; CytoD, cytochalasin D; DMSO, dimethyl sulfoxide; EGTA, ethylene glycol tetraacetic acid; LM, lamellum; LP, lamellipodium; MBL, Marine Biological Laboratory; PBS, phosphate-buffered saline, shRNA, short hairpin RNA; SIM, structured illumination microscopy; SMIFH2, small molecule inhibitor of formin homology domain 2; TEM, transmission electron microscopy.

Leiber *et al.*, 2013). All of these studies have supported the general conclusion that the Arp2/3 complex is critical for the generation and maintenance of the overall structure and dynamics of the LP. Specific studies have highlighted the complex's importance for activities such as cell spreading (Nicholson-Dystra and Higgs, 2008; Suraneni *et al.*, 2012; Wu *et al.*, 2012), response to the extracellular matrix (Wu *et al.*, 2012), chemotaxis (Suraneni *et al.*, 2012; Wu *et al.*, 2012), retrograde flow (Henson *et al.*, 2009; Yang *et al.*, 2012; Koestler *et al.*, 2013), and the modulation of other important LP actin cytoskeletal regulatory proteins, namely capping protein and cofilin (Koestler *et al.*, 2013). Despite these efforts, a number of fundamental questions remain about the precise nature of the structural organization and mechanism of polymerization of the actin cytoskeleton in Arp2/3 complex–inhibited cells (Koestler *et al.*, 2013).

In the present study, we use live-cell and fluorescence-based localization light microscopy and transmission electron microscopy (TEM) of cytoskeletal replicas to examine the effects of Arp2/3 complex inhibition on the LP actin cytoskeleton in sea urchin coelomocytes. These cells represent an exceptional experimental model, given their extraordinarily broad and Arp2/3 complex–rich LP region, exaggerated actin-based centripetal flow across the entire diameter of the cell, and extreme flatness and optical clarity, allowing for direct observation of the actin cytoskeleton in unmanipulated cells. Our studies on coelomocytes suggested that Arp2/3 complex activity is crucial for structuring the LP actin network (Henson *et al.*, 1999; 2009), for the generation of the pushing-force component of retrograde flow (Henson *et al.*, 1999, 2003), and for the closure of cytoplasmic wounds (Henson *et al.*, 2002). The present study builds on our previous work with the drug BDM, which induced delocalization of the Arp2/3 complex from the LP in coelomocytes (Henson *et al.*, 2009), a result reported initially in mammalian cells (Yarrow *et al.*, 2003). In addition, we extend the current literature through an examination of the short-time-scale transformation of the ultrastructural organization of actin in coelomocytes being both treated and washed out from the specific Arp2/3 complex inhibitor CK666, as well as the characterization of actin structure during the spreading of Arp2/3-inhibited cells. Furthermore, we examine specific features of previous studies in order to determine their relevance with regard to the coelomocyte system. These include the effect of CK666 on LP actin structure, retrograde flow rates (Yang *et al.*, 2012; Koestler *et al.*, 2013), and myosin II distribution (Koestler *et al.*, 2013). Furthermore, we initiate the process of defining the LP-specific roles of nucleators other than the Arp2/3 complex through the use of the small-molecule inhibitor of formin homology domain 2 (SMIFH2; Rizvi *et al.*, 2009) in CK666-treated cells. Finally, we compare the results in coelomocytes with those in other cells with broad LP regions, namely fish keratocytes and *Drosophila* S2 cells.

Our results illuminate the ultrastructural details of the significant transformation in the LP actin cytoskeleton that accompany Arp2/3 complex inhibition and recovery. They suggest that transverse arcs of elongate actin filaments are a universal feature of cells in which the Arp2/3 complex is inhibited and that these arcs may represent a class of filaments that are nucleated by formins. In addition, Arp2/3 inhibition significantly slows centripetal flow and the cell spreading process and induces a novel actin structure in spreading cells. Furthermore, although we observed the limited extension of myosin II distribution from the cell center in coelomocytes, we did not see clear evidence of myosin II transport into the former LP region. Finally, we document that CK666 treatment of coelomocytes in suspension induces a radical lamellipodial-to-filopodial shape change. Our results emphasize the major role that the Arp2/3 complex plays in helping organize actin architecture in cells and suggest that transverse actin arcs represent an integral component of LP structure that may be nucleated through the action of formin-like proteins and act as mother filaments during the dendritic nucleation process..

RESULTS

Arp2/3 inhibition dramatically alters LP actin organization

Live-cell imaging of the actin cytoskeleton with digitally enhanced phase contrast microscopy (Figure 1) and fluorescence labeling of actin filaments via phalloidin (Figure 2, A and E–G, and Supplemental Figure S1) or anti-actin antibodies (Figure 2, B–D) in fixed cells revealed that treatment with the Arp2/3 inhibitor CK666 led to two overlapping phenotypes, both involving the replacement of the dendritic array of actin with assemblages of elongate filaments. These phenotypes represented the two most typical morphologies of a spectrum of responses in the cells. The most frequent was the transverse actin arc form, in which the LP actin network was replaced with a series of actin arcs oriented parallel to the cell membrane that were generated by a process resembling delamination from the membrane's cytoplasmic face and subsequently underwent centripetal flow (Figures 1, A and B, 2, B, C, and E; Supplemental Figures S1, C and D, S2C, and S4, A–E; and Supplemental Movies S1 and S3). A particularly detailed view of the stark differences between the actin dendritic array in control cells and the actin arcs in Arp2/3- inhibited cells is afforded by superresolution three-dimensional (3D) structured illumination microscopy (SIM) of phalloidin-labeled cells (Supplemental Figure S1). The SIM images highlight the changes that CK666 treatment generated in actin structural organization not just within the LP, but also in the lamellar (LM) and perinuclear regions of the cells (Supplemental Figure S1). Note that LP-region actin arc-like bundles were also induced in cells treated with the Arp2/3 complex inhibitor CK869, which works via a different molecular mechanism than CK666 (Nolen *et al.*, 2009), and that actin structure in coelomocytes treated with dimethyl sulfoxide (DMSO; drug solvent) or the inactive control molecule CK689 were indistinguishable from untreated cells (Supplemental Figure S3).

CK666 treatment also produced another, less common phenotype, one dominated by filopodia in the altered LP region (Figures 1C and 2, D and F, and Supplemental Movie S2). The elongate bundles of actin in the filopodia were oriented perpendicular to the plasma membrane and imbedded in an array of orthogonally oriented filaments similar to those seen in the actin arcs (Figures 1C and 2, D and F). In some instances, the filopodial extension stimulated by drug treatment resulted in a slight expansion of the cell area, suggesting an increase in protrusive activity (Figures 1C and 2F). Axis-independent polarization microscopy of live cells indicated that both the filopodia and actin arcs exhibited birefringence consistent with arrays of aligned filaments (Supplemental Figure S2, A–C). The CK666 effect on coelomocytes was readily and rapidly reversible using washes with control buffer, which resulted in the initiation of a new dendritic network of actin at the periphery that progressed inward, pushing the CK666-generated actin array ahead of it (Figures 1B and 2G and Supplemental Movies S1 and S3). Once in the cell center, the drug-influenced actin cytoskeleton was dismantled, and eventually cells washed out of CK666 returned to completely normal morphology (Figure 1B and Supplemental Movie S1).

TEM imaging of coelomocyte cytoskeletal replicas allowed for fine temporal resolution analysis of the effects of both CK666 treatment and washout on the ultrastructure of the coelomocyte actin cytoskeleton (Figure 3). Within 30 s of CK666 addition, the very dense dendritic array of branched filaments characteristic of the LP region of control cells (Figure 3, A and C) was replaced by a less dense assemblage of longer filaments, with many oriented

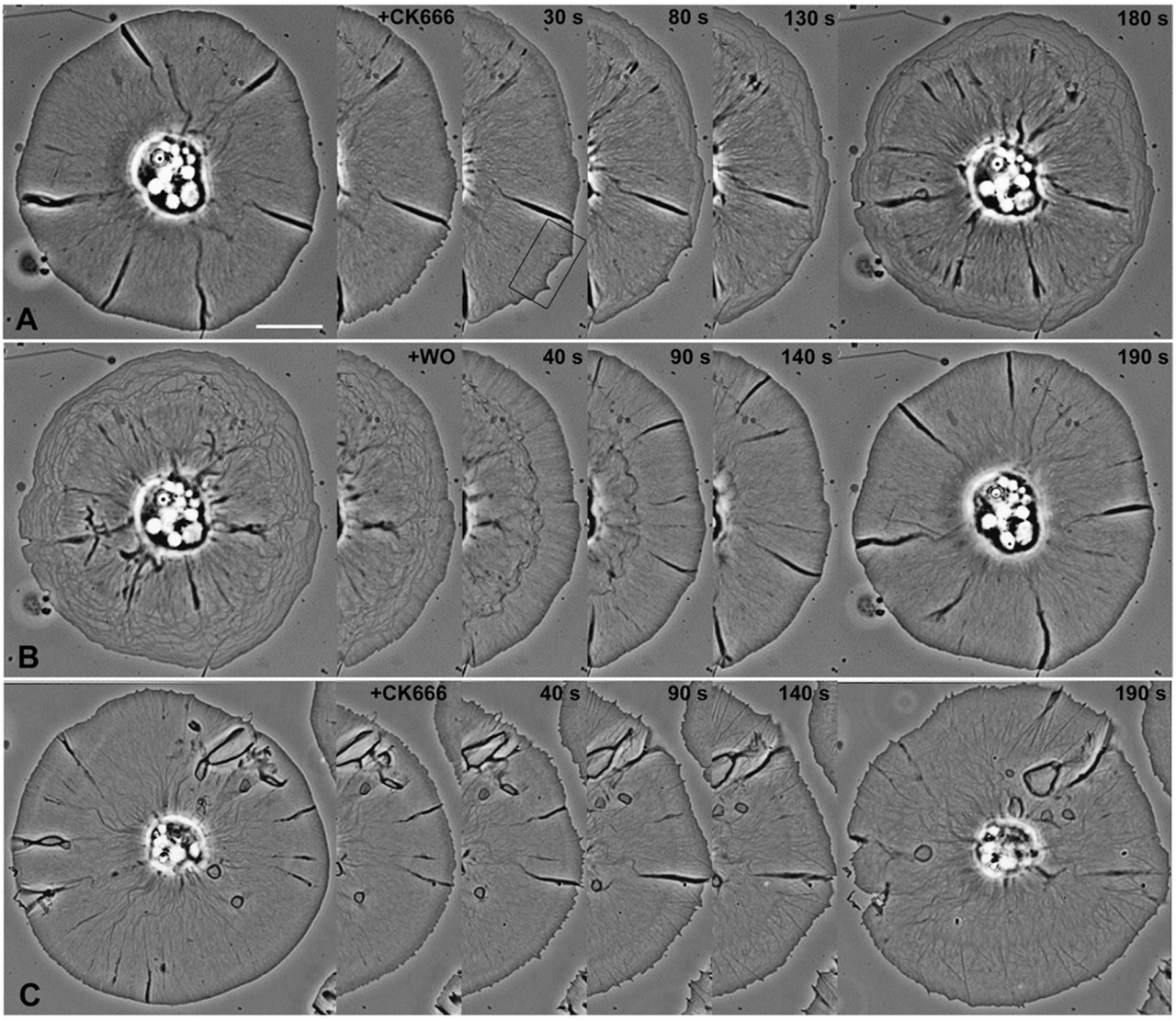

FIGURE 1: Arp2/3 complex inhibition radically transforms the coelomocyte LP actin cytoskeleton. Live-cell phase contrast images from two digital movies shows that 100 µM CK666 treatment results in two basic phenotypes—a more common, transverse arc form (A, B) and a less common, filopodial form (C). In each case, the dense dendritic array of the control cells is replaced with less dense assemblages of elongate filaments. The effects of CK666 are readily reversible, as illustrated in the sequential wash out (+WO) images in B, in which the actin arcs are completely replaced by the control actin organization. The box in the 30-s post-CK666 treatment image in A denotes a region of the cell that generates a response analogous to that seen in the TEM image in Figure 3D. Bar, 10 µm; magnifications of A–C are equivalent.

diagonally or parallel to the membrane (Figure 3D). In addition, the tips of bundles of actin filaments are seen to be associated with small, pyramid-shaped protrusions on the membrane (Figure 3D), which were also seen in live-cell (Figure 1, A, boxed region of the 30-s image, and C) and fluorescence microscopy (Figure 2D). Consistent with light microscopic imaging (Figures 1, A and B, and 2E, and Supplemental Figure S1), TEM also revealed that with increasing time of CK666 treatment, the peripheral actin arcs became more and more dominant and less dense (Figure 3, E and F) and tended to occupy an increasing percentage of the diameter of the cell (Figure 3B). The arcs consisted of lose bundles of elongate and typically unbranched actin filaments (Figure 3F) and were ultrastructurally similar to the actin arcs produced by treating coelomocytes with BDM (Henson *et al.*, 2009). TEM imaging of CK666 washout showed that within seconds, the cell edge produced a control-like assemblage of dendritic actin that displaced the actin arc structural organization centripetally and that the dendritic array grew wider over time (Figure 3, G and H). It is important to note that close examination of the newly forming dendritic network in the washed-out cell replicas revealed the existence of tangentially oriented elongate actin filaments (particularly noticeable in Figure 3H) that were also present, although less obvious, in the dense LP network of control cells (Figure 3C). Given that the washout of the CK666 effect was so rapid, we were careful to include appropriate drug concentrations in all initial fixative and extraction buffers to prevent unwanted recovery of the control condition.

Arp2/3 inhibition significantly slows actin-based centripetal flow

Sea urchin coelomocytes in culture are characterized by persistent and robust centripetal flow (Henson *et al.*, 1999, 2002, 2009), and analysis of centripetal flow was performed to determine whether

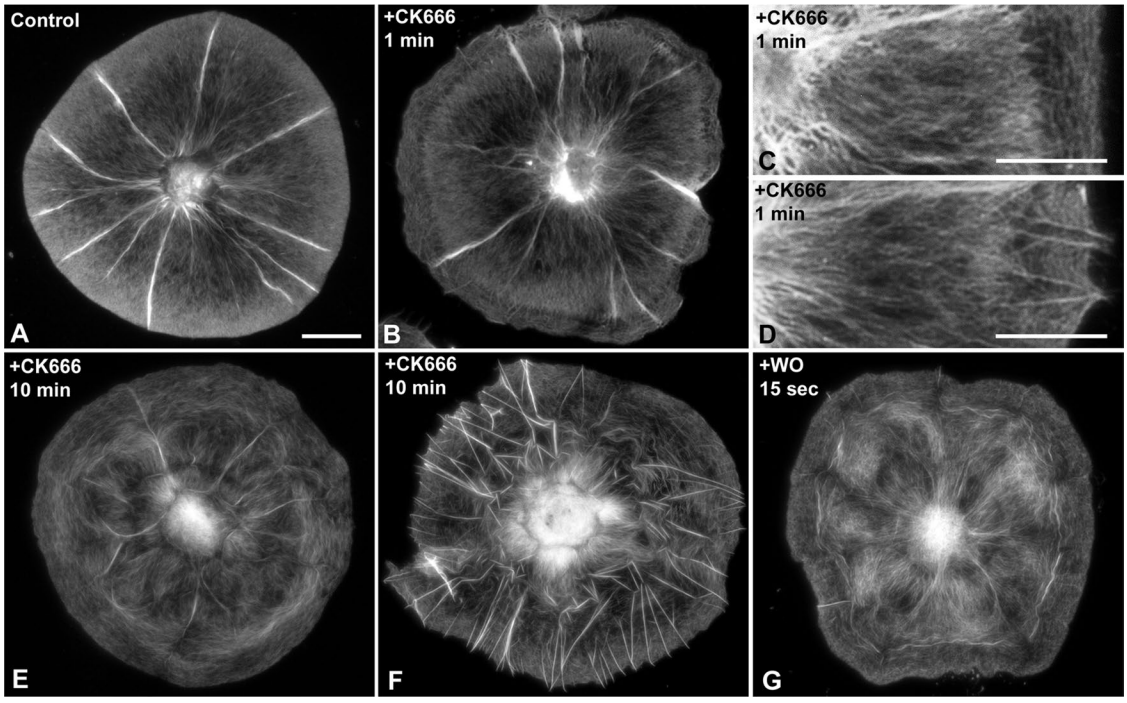

FIGURE 2: Fluorescence staining of actin in Arp2/3 complex–inhibited coelomocytes. Fluorescent phalloidin (A, E–G) and actin antibody staining (B–D) of cells treated with 100 μM CK666 corroborates the live-cell imaging in depicting the transition of the control dendritic network (A) into the actin arcs (B, C, E) and actin filopodia (D, F) present in CK666-affected cells. Washing the cells out of CK666 with control buffer (+WO; G) rapidly reestablishes the control dendritic array at the cell edge, which then moves centripetally. Bar, 10 μm; magnifications of A, B, and E–G are equivalent.

Arp2/3 inhibition altered the speed of the movement (Figure 4, A–E and K). Measurements of 20 different cells before and after drug treatment indicated that coelomocyte centripetal flow slowed significantly ($p < 0.001$) when treated with CK666 and increased significantly ($p < 0.001$) when washed out of the drug (Figure 4, K and L). The significant effect of Arp2/3 complex inhibition underscores the importance of its function in the maintenance of the rapid centripetal flow rates characteristic of the LP region. To verify that actin polymerization was indeed responsible for the production and flow of the CK666-induced arcs, we treated cells initially with CK666, followed by a combined treatment of CK666 plus the actin polymerization–disrupting drug cytochalasin D (CytoD). Treatment with CytoD resulted in the gradual arrest of arc formation and a clearing of the cortical region due to the retraction of the central cytoskeleton as a consequence of continued actomyosin contraction (Figure 4, F–J). During this retraction, a minority of arcs maintained a single point of contact with the membrane at the cell edge (Figure 4J). We previously reported on CytoD's ability to produce cleared fringes and central cytoskeletal contraction in coelomocytes (Henson *et al.*, 2002, 2009), a response that is reminiscent of the cytochalasin phenotype originally demonstrated in *Aplysia* growth cones (Forscher and Smith, 1988).

Arp2/3 complex inhibition alters the distribution of the complex and myosin II

Immunolocalization of actin and Arp3 indicated that CK666 treatment resulted in an overall decrease in Arp3 labeling, as well as loss of Arp3 signal from the LP region of cells displaying the actin arc phenotype (Figure 5, A–F). The validity of this change in localization is supported by images showing two adjacent cells in which strong dendritic actin and Arp3 labeling overlap is seen in one (left-hand cell in Figure 5, D–F), whereas strong actin arcs and weak Arp3 staining are seen in the other (right-hand cell in Figure 5, D–F). In addition, pixel intensity measurements of control (+CK689) and Arp2/3 complex–inhibited cells (+CK666 or +CK869) demonstrate a greatly diminished Arp3 localization signal in the latter cells (Supplemental Figure S4). In previous work, we demonstrated that Arp3 staining is delocalized from the edge of coelomocytes treated with BDM (Henson *et al.*, 2009). However, unlike the overall diminishment of the Arp3 label in cells treated with CK666, Arp3 staining is retained in the central cytoskeleton of the BDM-treated cells (see Figure 1 in Henson *et al.*, 2009). This suggests that CK666 eliminates the incorporation of the Arp2/3 complex from assembling actin filaments and also induces dissociation of the Arp2/3 complex from the previously formed dendritic actin cytoskeleton (also suggested by Yang *et al.*, 2012), whereas BDM selectively interferes with only the peripheral localization of Arp2/3 complex (a hypothesis that is also supported by some of our recent unpublished results comparing the effects of BDM and CK666).

In earlier work, we demonstrated that a centrally located array of actin and myosin II provides the contractile pulling force component of coelomocyte centripetal flow (Henson *et al.*, 1999, 2003, 2009). Therefore, as expected, control cells contained a tightly focused array of perinuclear myosin labeling (Figure 5, G–I). Treatment with CK666 resulted in a spreading of the myosin staining pattern (Figure 5, J–L) in concert with an overall relaxation of the actomyosin ring present in the cell center (as seen in the SIM-imaged, phalloidin-stained cells in Supplemental Figure S1, C and D), a response also seen in cells treated with BDM (Henson *et al.*, 2009). Note that in CK666-treated cells, the myosin II tended to localize in radially arranged ribs that serve as collection sites for the centripetal migration of actin arcs (Figure 5, J–L, and Supplemental Movies S1 and S3).

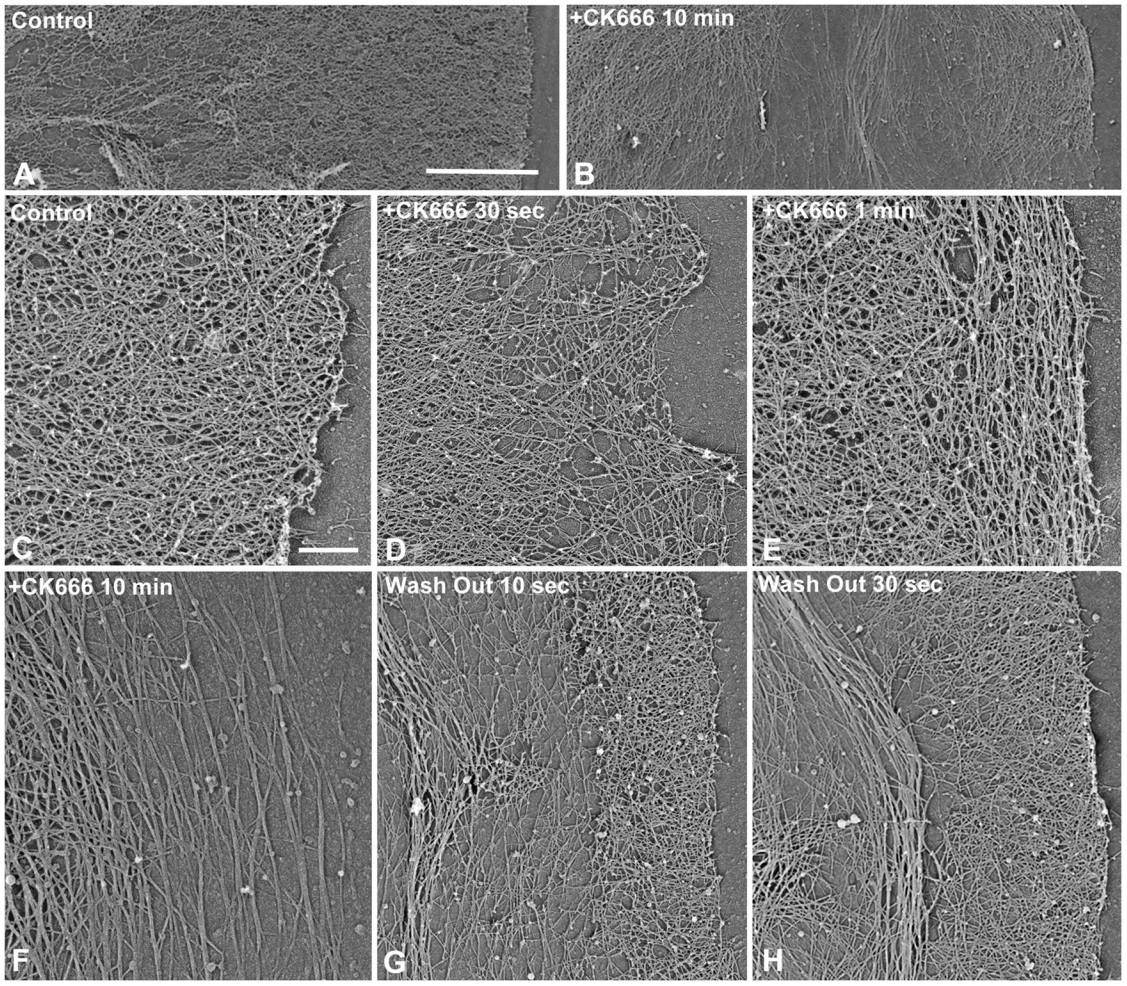

FIGURE 3: Ultrastructure of the alteration of actin organization during Arp2/3 complex inhibition. Control cells (A, C) contain a dense dendritic network of actin filaments in their LP region, which, upon treatment with 100 μM CK666, rapidly transitions to an array of less dense elongate filaments oriented diagonally and parallel to the membrane (D, E). The pyramidal projections seen in D are analogous to the similar structures apparent in the live-cell imaging in the boxed region of the 30-s image in Figure 1A. Over time, the transverse actin arcs become apparent, decrease in density, and tend to occupy more of the cell diameter (B, F) and consist of loosely affiliated and highly elongate actin filaments. Washout of CK666 (G, H) results in the immediate restart of the dense dendritic actin network at the cell edge, and this pushes centripetally, and elongate actin filaments oriented at low angles to the membrane are apparent within this network. Bar, 5 μm (A), 1 μm (C); magnifications of A, B, and C–H are equivalent.

Although the myosin distribution did spread out as a result of CK666 treatment, there was little evidence of the transport of myosin to the cell edge as reported by Koestler *et al*. (2013).

Arp2/3 inhibition in suspended coelomocytes drives a lamellipodial-to-filopodial shape change and alters the dynamics and structure of actin during spreading

Early studies on coelomocytes demonstrated that these cells undergo a dramatic lamellipodial-to-filopodial shape change when challenged in suspension with hypotonic shock (Edds, 1979; Otto *et al.*, 1979) or treatment with calcium ionophore (Henson and Shatten, 1983; Hyatt *et al.*, 1984). Arp2/3 complex inhibition in other cell types has been shown to be associated with an increase in filopodia (Nicholson-Dystra and Higgs, 2008; Suraneni *et al.*, 2012; Wu *et al.*, 2012; Koestler *et al.*, 2013), and we saw this to a limited degree in attached cells treated with CK666 (Figures 1C and 2, D and F). In contrast, treatment of coelomocytes in suspension resulted in the transformation of the cells from a form possessing a number of lamellipodia to one containing numerous elongate filopodia (Figure 6, D and I–K, and Supplemental Figure S2, D and E), and, as part of these experiments, we investigated the ability of the CK666-treated cells to spread on a substrate. Consistent with a previous study using a short hairpin RNA (shRNA) depletion approach in mammalian fibroblasts and lymphocytes (Nicholson-Dystra and Higgs, 2008), we found that CK666-based Arp2/3 inhibition slowed the progress of cell spreading relative to control cells (Figure 6, A–J and L). In addition, Arp2/3 complex inhibition greatly altered the structural organization of actin in the spreading cells (Figure 6, A–J). Filopodia from control coelomocytes typically return to their lamellipodial form during the spreading process, as was seen when cells transformed to the filopodial form by CK666 treatment in suspension were allowed to attach briefly to a coverslip and then washed out of the drug using control buffer (Figure 6, A–C, G, and H). In these control cells, the filopodia were consumed by the rapid spreading out of numerous LPs containing the expected dendritic array of actin filaments, as demonstrated by phalloidin staining (Figure 6, A and C) and TEM

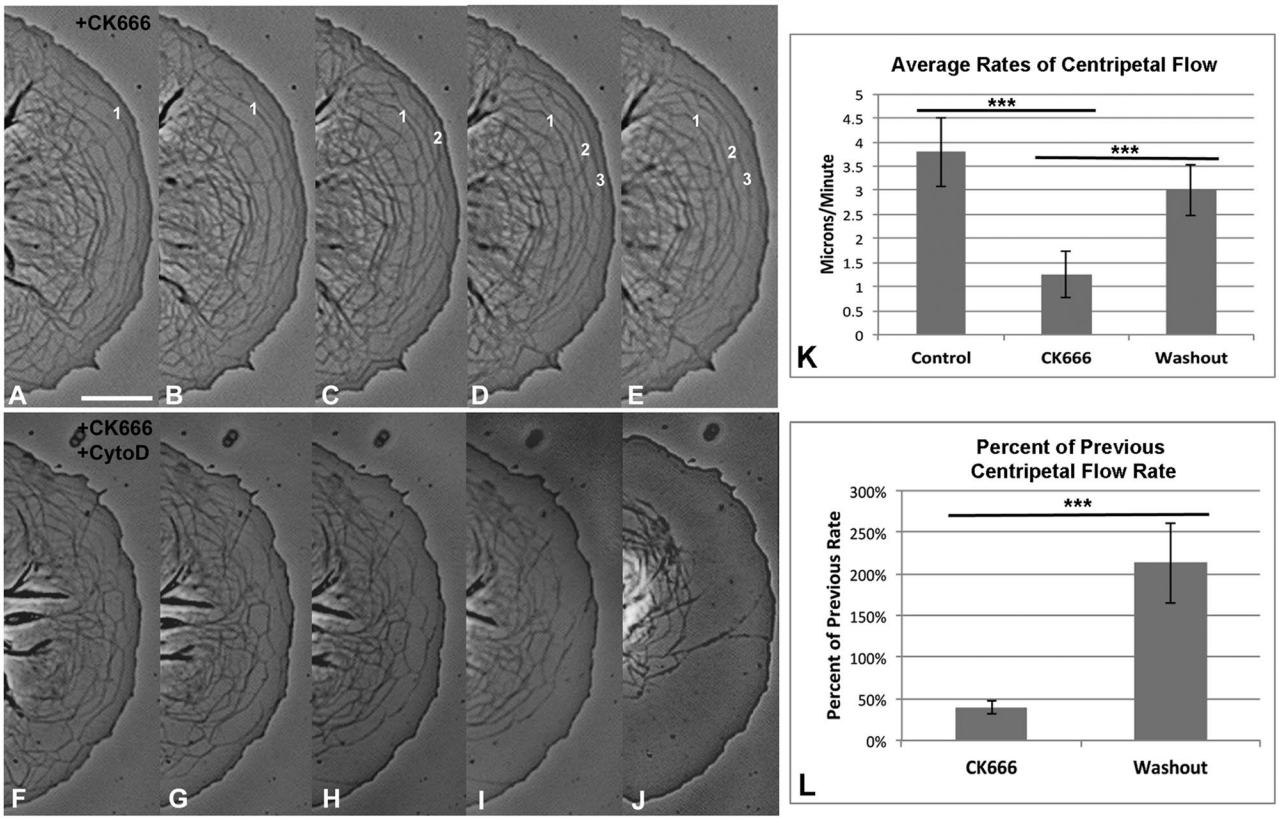

FIGURE 4: CK666-induced actin arcs delaminate from the cell edge, undergo decreased centripetal flow, and are arrested by CytoD treatment. Phase contrast digital movies reveal the delamination-like generation of actin arcs in a cell treated with 100 μM CK666 (A–E; 50 s between images; 1–3 mark three consecutive arcs) and that arc production can be arrested by treatment with 500 nM CytoD (F–J; time between images is 60 s for F–I and 180 s for I to J). Quantification of average (K) and percentage previous (L) centripetal flow rates shows that CK666 treatment significantly slows centripetal flow. ***Statistically significant differences at the $p < 0.001$ level. Bar, 10 μm; magnifications of A–J are equivalent.

(Figure 7, A–C). In contrast, cells spreading in the presence of CK666 showed that their LP regions contained actin arcs (Figures 6, D–F and J, and 7, D–F) similar to that seen in drug-treated attached cells (Figures 1–4). Moreover, these structures were birefringent, as detected by polarizing microscopy (Supplemental Figure S2F), arose from the cell edge, and underwent centripetal flow (Supplemental Movie S4). In addition, unlike the smooth process of spreading exhibited by the LPs in the control cells, the edges of CK666-treated cells tended to undergo intermittent/jerky protrusive activity (Supplemental Movie S4). In instances of the spreading around points at which filopodia touched the substrate, the actin arcs formed an unusual concentric circle pattern as seen in phalloidin labeling (arrow in Figure 6F) and TEM (Figure 7, F and H). These images suggested that the actin reorganization accompanying the spreading of CK666-treated cells was fundamentally different from controls and did not involve the formation of LP-like regions with dendritic networks of filaments. They also indicate that coelomocytes retain the ability to spread even in the absence of the ability to form a conventional LP architecture.

Formin inhibition arrests the CK666-induced production of actin arcs

To test our working hypothesis that the CK666-induced actin arcs are the result of formin-facilitated actin polymerization, we treated coelomocytes initially with CK666, followed by a mixture of CK666 plus SMIFH2, which is described in Risvi *et al*. (2009). SMIFH2 treatment resulted in the initial slowing of arc centripetal flow and the eventual arrest of their generation from the cell edge (Supplemental Movie S5 and Figure 8A). Live-cell (Figure 8B), phalloidin staining (Figure 8C), and TEM (Figure 8, D and E) images of the effect of formin inhibition alone on control cells showed that this drug leads to a cell-wide disruption in actin architecture in which the effected cells displayed patches of dense and less dense actin networks. This patchy distribution of actin networks was similar to that reported by Yang *et al*. (2007) in TEM images of mammalian cells in which formin/mDia was depleted by shRNA treatment. Note that normal actin organization could be restored in coelomocytes washed out of the SMIFH2 drug (Supplemental Movie S6 and Figure 8, F–I).

Other cell types with broad LP regions—fish keratocytes and *Drosophila* S2 cells— generate actin arcs on Arp2/3 complex inhibition

The central nature of actin arcs in the coelomocyte response to Arp2/3 complex inhibition led us to postulate that other cell types containing broad LP regions would respond in a similar manner. We initially focused on fish keratocytes and found that CK666 treatment slowed or halted keratocyte migration (unpublished data) and produced actin arcs in the LP region that were visible with phalloidin staining (Figure 9, A–H) and were reminiscent of the arcs present in coelomocytes. During the course of these experiments, we learned of recent work that also reported the presence of actin filaments parallel to the membrane in fish keratocytes in which the Arp2/3

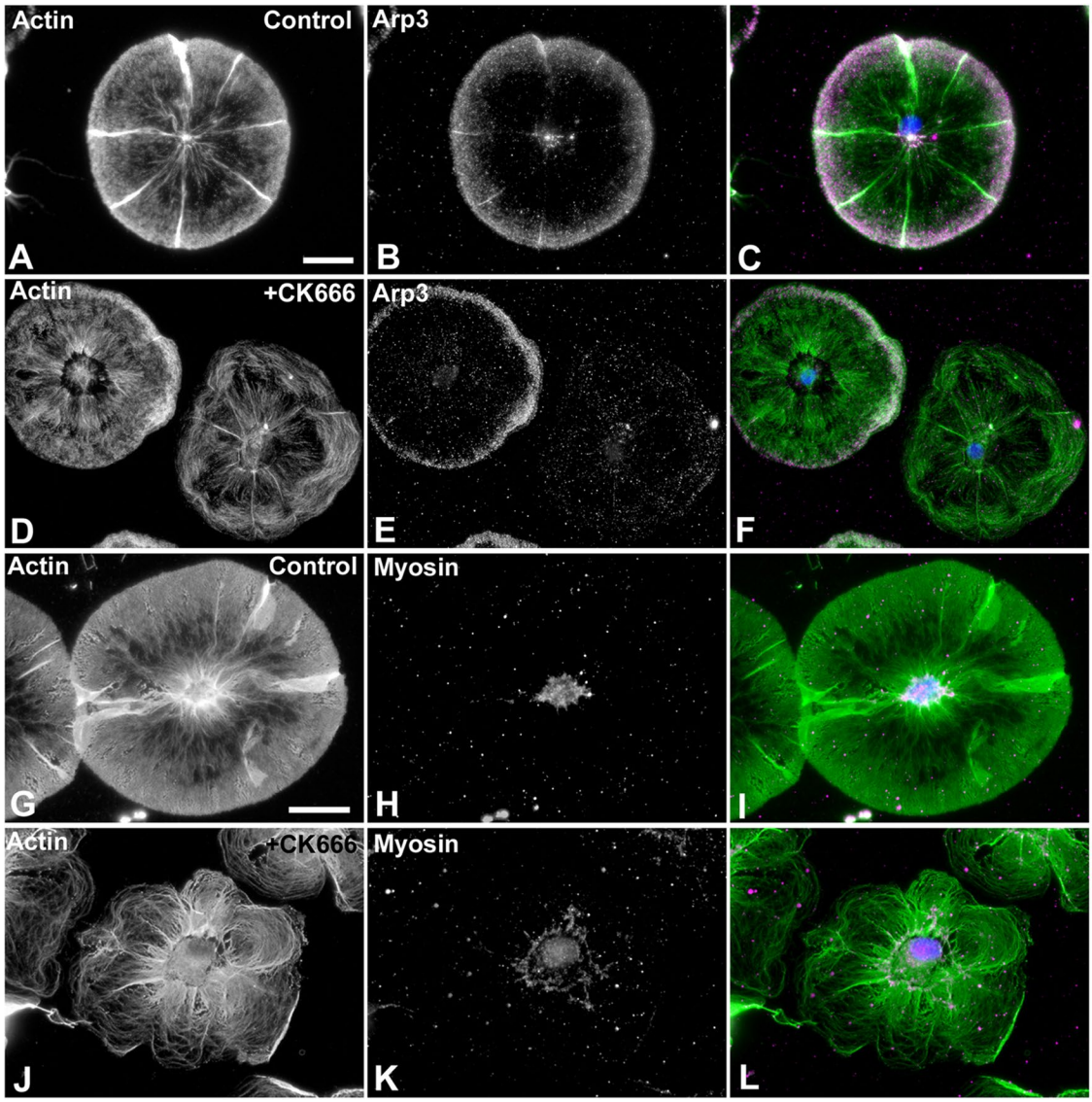

FIGURE 5: The distributions of Arp2/3 complex and myosin II are altered by CK666 treatment. Immunofluorescence labeling of actin (A, D, green in C and F) and Arp3 (B, E, magenta in C and F) in control (A–C) and 100 µM CK666–treated (D–F) cells shows that the dense Arp3 labeling apparent in control cells is substantially decreased in cells containing the CK666-induced actin arc phenotype (right-hand cell in D–F). Staining for actin (G, J, green in I and J) and myosin II (H, K, magenta in I and L) in control (G–I) and 100 µM CK666–treated (J–L) cells demonstrates that the tightly compacted perinuclear myosin II ring apparent in control cells becomes more spread in cells exhibiting a CK666-induced actin arc phenotype. Nuclei in C, F, I, and L are labeled blue. Bar, 10 µm; magnifications of A–F and G–L are equivalent.

complex was inhibited by either treatment with CK666 (Koestler *et al.*, 2013; Lieber *et al.*, 2013) or WCA-based sequestration (Koestler *et al.*, 2013). In other experiments, we tested the effect of CK666 treatment on *Drosophila* S2 cells and discovered that they also respond to Arp2/3 complex inhibition by the generation of LP actin arcs (Figure 9, I–P). These results with two cell types widely separated phylogenetically underscore the universality and significance of the actin arc response to Arp2/3 inhibition in cells containing wide LP regions.

DISCUSSION

In the present study, we demonstrate that pharmacological inhibition of the Arp2/3 complex in sea urchin coelomocytes leads to 1) a radical restructuring of the LP actin cytoskeleton, with the associated generation of actin arcs from the cell edge, 2) a significant decrease in centripetal flow, 3) a limited redistribution of the perinuclear myosin II distribution, 4) a transformation of suspended cells from a lamellipodial to a filopodial form, and 5) a slowing of the cell spreading process and a novel alteration in the actin structure of spreading cells. We also show that a formin inhibitor arrests the production of the actin arcs induced by Arp2/3 complex inhibition. Each of these main results will be discussed in the context of the literature.

A number of previous studies on several different cell types demonstrated the presence of elongate actin filaments oriented parallel to the plasma membrane, using TEM imaging of cells in which Arp2/3 complex activity had been reduced using a variety of approaches (Steffan *et al.*, 2006; Korobova and Svitkina, 2008; Wu *et al.*, 2012; Yang *et al.*, 2012; Koestler *et al.*, 2013; Lieber *et al.*, 2013). The presence of the elongate filaments in these

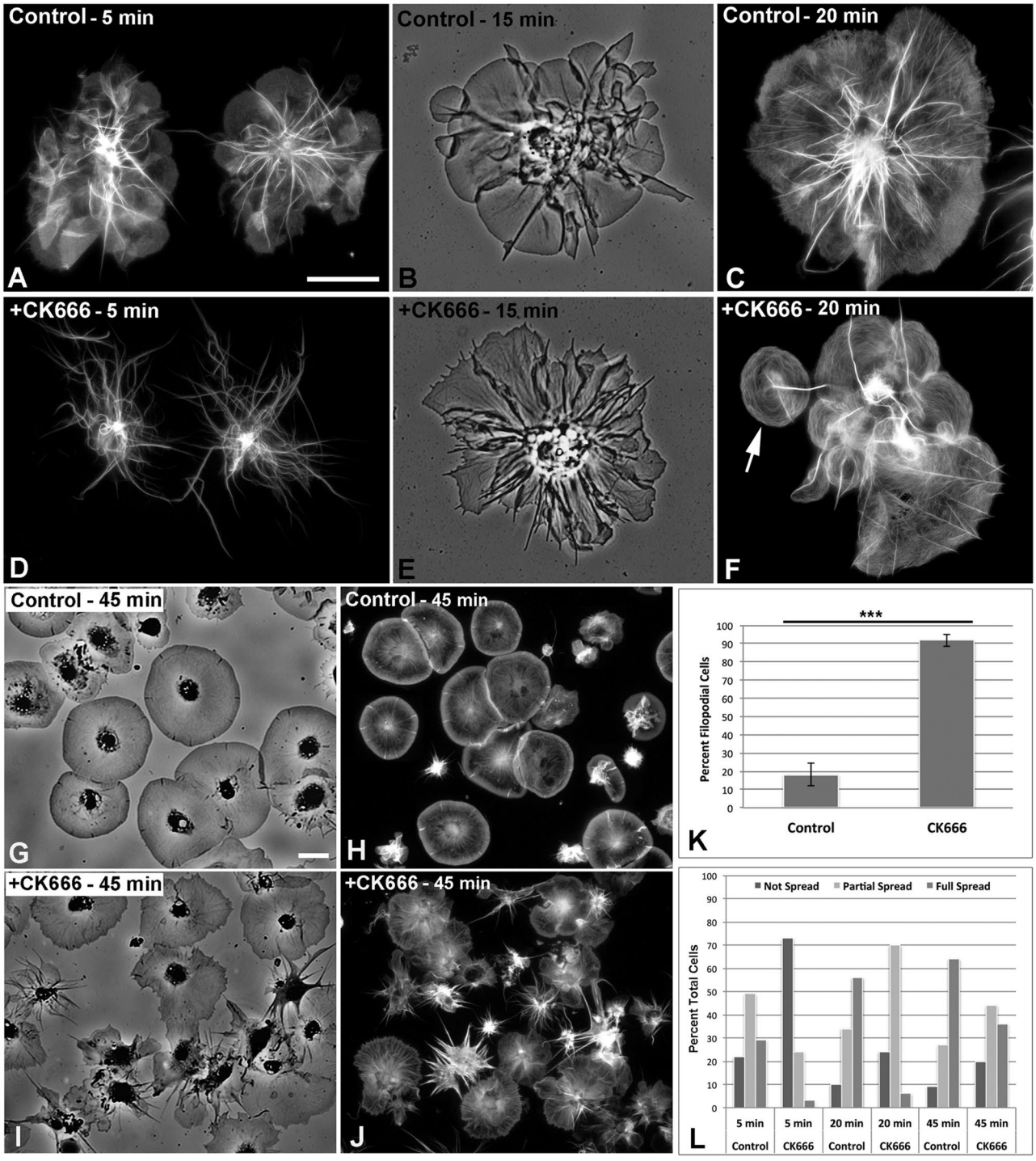

FIGURE 6: Arp2/3 complex inhibition retards the process of coelomocyte spreading and induces a novel actin organization. Cells treated in suspension with 100 μM CK666 undergo a lamellipodial-to-filopodial shape change, as seen when allowed to settle for 5 min and stained with phalloidin (D). In contrast, cells washed out of the drug just after substrate attachment and imaged 5 min later (A) show numerous LP-like spreading regions. With increasing time post settling (B and E, 15 min; C and F, 20 min; G–J, 45 min), control cells (B, C, G, H) spread into the typical discoidal morphology, with prominent LP dendritic arrays, whereas the spreading CK666-treated cells (E, F, I, J) have processes containing noticeable actin arcs and numerous filopodia. In these cells, the processes produced in regions of spreading from filopodia making focal substrate contacts can contain novel concentric circle patterns of actin arcs (arrow in F). Quantification shows that CK666 treatment of coelomocytes in suspension induces a significantly larger number of filopodial cells than control treatment with CK689 (K; $p < 0.001$) and that control/washout cells spread faster than cells kept in the presence of the drug (L). Bars, 10 μm; magnifications of A–F and G–J are equivalent.

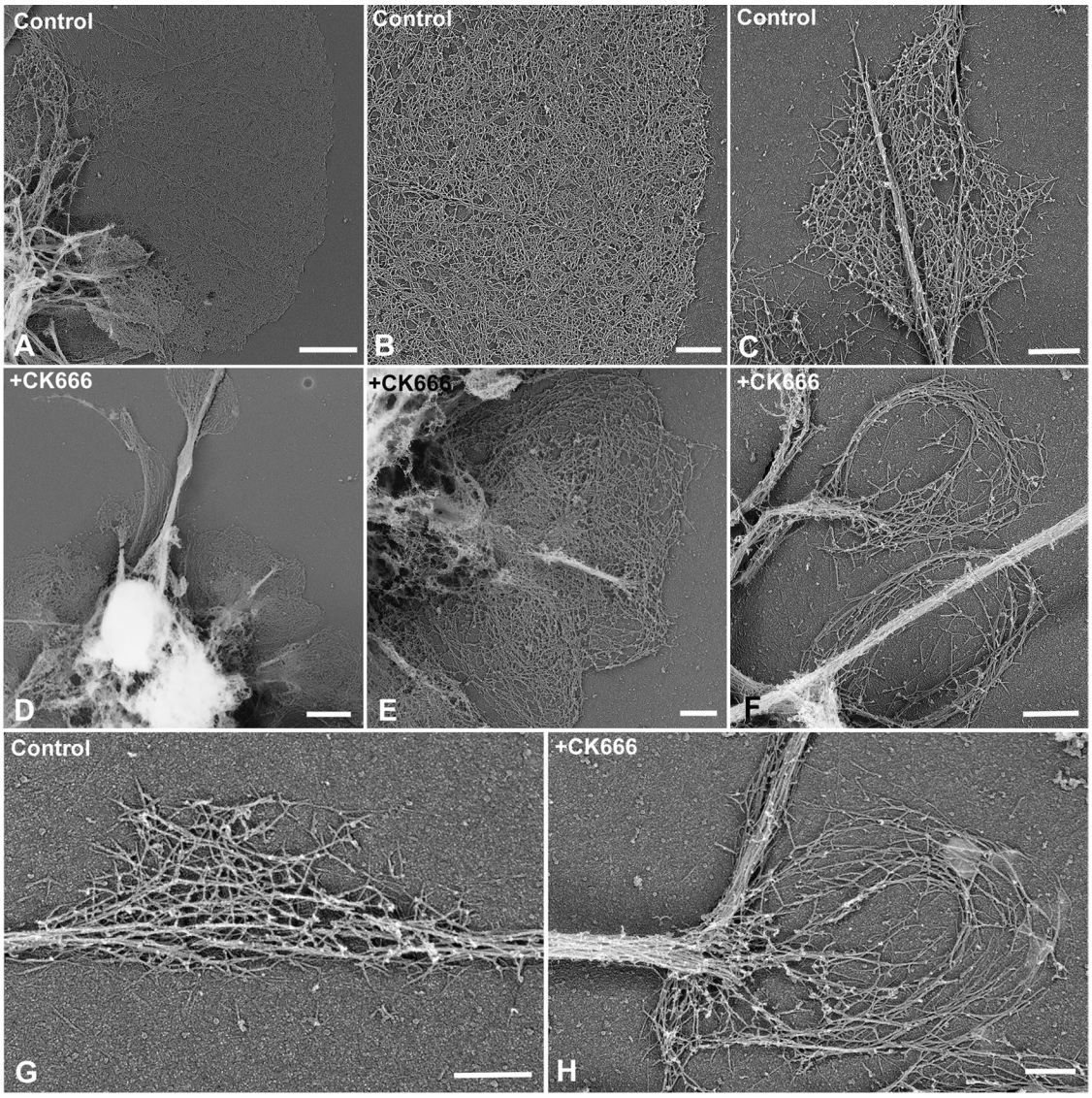

FIGURE 7: Ultrastructural organization of actin in control and Arp2/3 complex–inhibited spreading cells. TEM imaging of control/washout cells settled for 15 min (A–C, G) shows that the spreading peripheral regions contain the expected LP-like dendritic actin network (A, B). In contrast, cells spreading in the presence of 100 μM CK666 for 15 min (D–F, H) possess more- limited spread regions containing actin arcs of elongated filaments (D, E). In spreading filopodial regions, control cells show evidence of small regions of dendritic actin arrays (C, G), whereas CK666-affected cells display actin arcs arrayed in unusual concentric circle patterns (F, H). Bars, 2 μm (A, D), 0.5 μm (B, C, E–H).

various cell types was often relatively subtle and difficult to visualize using light microscopy, whereas in the coelomocyte, the edge-associated elongate actin filaments form well-defined arc-like structures that can be clearly visualized in live, unlabeled cells (Figures 1 and 4, Supplemental Figure S2, and Supplemental Movies S1–S3). Our speculation is that the uniquely broad nature of the LP region of coelomocytes allows for this exaggerated response to CK666 treatment, and we show that actin arcs are induced in other cell types that also contain broad LP regions, namely fish keratocytes and *Drosophila* S2 cells (Figure 9). We previously reported that actin arcs were induced in coelomocytes by treatment with the drug BDM (Henson *et al.*, 2009), and the replication of this BDM phenotype with the specific inhibitor CK666 supports our hypothesis that at least one of the indirect effects of the drug BDM is to interfere with Arp2/3 complex activity/localization.

An important question about the CK666-induced actin arcs in coelomocytes is whether they are similar to the transverse actin arcs long known to be present in the LM region of many other cell types (Heath, 1983; Small and Resch, 2005; Hotulainen and Lappalainen, 2006; Burnette *et al.*, 2011). These structures tend to arise proximal to the LP/LM interface and are characterized by tightly bundled actin filaments with associated α-actinin and myosin II, features that are not shared by the CK666-induced coelomocyte arcs. The CK666-associated arcs may represent an immature form of organization, given that arcs have been shown to evolve over the time between their initial polymerization and maturation into a contractile bundle (Hotulainen and Lappalainen, 2006). However, control coelomocytes lack obvious transversely oriented actin arcs, and instead their interior LM region is dominated by the presence of large, radially oriented bundles of elongate actin filaments (Figures 1A and 2A and Supplemental Figure S1, A and B) that are not associated with

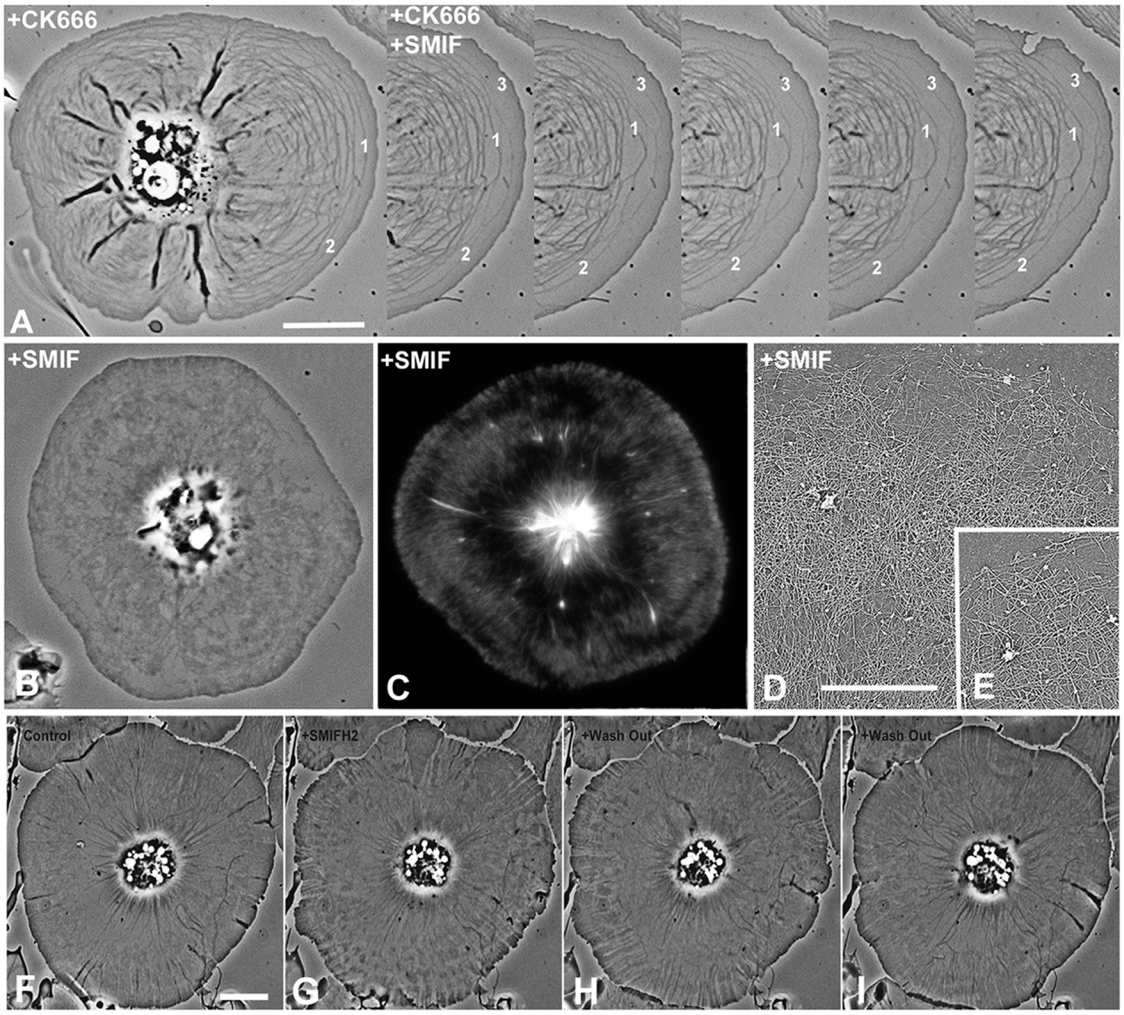

FIGURE 8: The generation of actin arcs in Arp2/3 complex–inhibited cells is arrested by treatment with the formin inhibitor SMIFH2. Phase contrast digital movie of a cell treated with 100 μM CK666 followed by treatment with CK666 plus 5 μM SMIFH2 (A; time between the first and second images is 10 s and between subsequent images is 60 s). Arc generation and centripetal movement continued briefly after SMIFH2 application (note movement of arcs 1 and 2 and production of arc 3) and then was clearly arrested. Treating control cells with 2.5–5 μM SMIFH2 (B–E) for 10 min resulted in the patchy, discontinuous distribution of actin networks as seen in live-cell phase contrast (B), fluorescent phalloidin staining of actin (C), and TEM imaging (D, E). A control cell (F) treated with 2.5 μM SMIFH2 for 10 min (G) shows disruption in the actin cytoskeleton. Washing out the drug for 2 (H) or 15 min (I) restores the control actin structural organization (I). Bars,10 μm (A, F), 5 μm (E); magnifications of A–C and F–I are equivalent.

myosin II in control cells (Figure 5; Henson *et al.*, 1999, 2003). We speculate that coelomocyte LP arcs are not equivalent to the arcs present in the LM of other cells and instead represent elongate filaments typically formed in the LP region of control cells but are hidden within the high-density dendritic actin network (Figure 3). Koestler *et al.* (2008) reported that elongate actin filaments parallel to the cell edge and similar to coelomocyte arcs were most prominent in areas of cells not undergoing active protrusion.

An intriguing possibility is that the arcs of parallel actin filaments seen in CK666-treated coelomocytes may represent the "mother" filaments onto which the Apr2/3 complex must bind to generate side branches (Gupton *et al.*, 2007; Yang *et al.*, 2007). Vinzenz *et al.* (2012) used a single cell wounding approach in mammalian cultured cells—first developed in our lab using coelomocytes (Henson *et al.*, 2002)—to demonstrate that Arp2/3 complex–dependent branches form off of layers of elongate filaments oriented parallel to the wound edge membrane, and these filament layers are reminiscent of the CK666-induced arcs in coelomocytes.

In terms of the actin polymerization mechanism responsible for generating arcs, we demonstrate that a formin inhibitor (SMIFH2) arrests the production of the CK666-induced arcs in coelomocytes (Figure 8) and that the actin structural changes elicited by this inhibitor in coelomocytes resemble those seen in another study using shRNA against formin/mDia in mammalian cells (Yang *et al.*, 2007). In addition, Suraneni *et al.* (2012) demonstrated that formin/mDia proteins localized to the tips of filopodium-like structures in cells devoid of the Arp2/3 complex. Therefore it is possible that formin/mDia proteins are mediating the polymerization of the actin arcs, although Ena/VASP-like proteins (Bear and Gertler, 2009) could also be involved. With regard to arc motility, our previous work with BDM-induced arcs (Henson *et al.*, 2009) and present experiments with the CK666-treated cells suggest that myosin II contraction plays a role in their centripetal motility, consistent with other studies involving Arp2/3 inhibition (Yang *et al.*, 2012; Koestler *et al.*, 2013).

The significant decrease in centripetal/retrograde flow that we report for Arp2/3 complex–inhibited coelomocytes (Figure 4) is

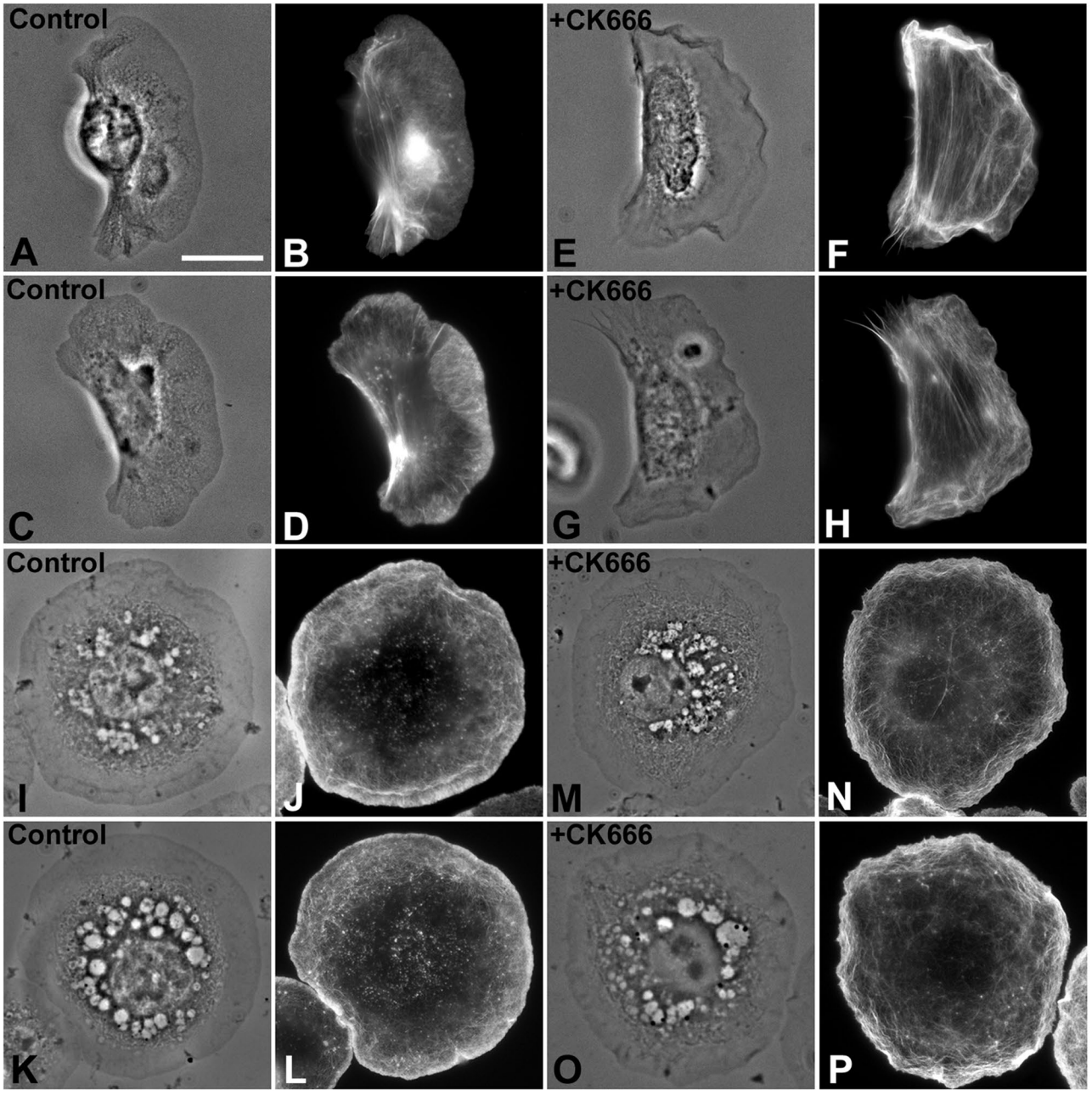

FIGURE 9: Inhibition of the Arp2/3 complex in fish keratocytes and S2 cells induces actin arc formation. Phase contrast (A, C, E, G) and fluorescent phalloidin (B, D, F, H) imaging of control (A–D) and 100 µM CK666–treated (E–H) fish keratocytes demonstrates that the drug transforms the LP region from a dendritic network into a collection of transverse, elongate filaments. A similar response is seen when control S2 cells (I–L) are treated with 100 µM CK666 (M–P), suggesting that actin arcs are a common feature of Arp2/3 complex inhibition in cells with broad LP regions. Bar, 10 µm; magnifications of A–P are equivalent.

consistent with previous studies using cultured mammalian fibroblasts (Koestler *et al.*, 2013) and neuronal cells (Korobova and Svitkina, 2008) but conflicts with the results of Yang *et al.* (2012) using *Aplysia* growth cones. This last study indicated that treating growth cones with CK666 resulted in the significant acceleration of retrograde flow and that the slowing of flow with CK666 treatment was only seen in cells pretreated with the myosin II inhibitor blebbistatin. The differential response of *Aplysia* growth cones and coelomocytes to Arp2/3 complex inhibition is not surprising, given the substantial differences in their actin cytoskeletal organization. The growth cones contain numerous edge-associated filopodia in their LP-equivalent P region (Yang *et al.*, 2012), whereas filopodia are rare in control coelomocytes (Figures 1–5). In the growth cones, CK666 treatment would spare the filopodia, and therefore increased flow might be expected as a result of a shift of actin polymerization from numerous edge-associated sites to fewer filopodial tips, and, in agreement with this idea, the filopodia in the CK666-treated cells do appear longer and more robust (Yang *et al.*, 2012). It is interesting that an older study demonstrated that BDM treatment of *Aplysia* growth cones also tended to result in the growth of filopodia (Lin *et al.*, 1996), suggesting that there might be some overlap in the effects of CK666 and BDM in growth cones similar to what we show for coelomocytes.

In terms of myosin II labeling, CK666 treatment of coelomocytes does induce a limited spreading of the myosin II array located in the center of control cells (see also Henson *et al.*, 1999, 2003), and this more widely distributed myosin II tends to concentrate along radial ridges in the cytoskeleton that correspond to collection sites for actin arcs (Figures 1, 4, and 5), where actomyosin contraction may be providing a pulling force for their centripetal movement. Koestler *et al.* (2013) report that in fibroblasts, Arp2/3 complex inhibition leads to myosin II patch movement from the LM to nearer the cell edge and distal of the former LM/LP boundary. In coelomocytes, myosin II does not associate with the CK666-induced actin arcs and does not appear to spread into the LP region, a result also reported in CK666-treated *Aplysia* growth cones (Yang *et al.*, 2012).

The LP region would be expected to be involved in the process of cells spreading out on a substrate, and earlier work in mammalian cells showed that depletion of the Arp2/3 complex does interfere with the spreading process (Nicholson-Dystra and Higgs, 2008; Suraneni *et al.*, 2012; Wu *et al.*, 2012). Our findings in coelomocytes confirm these results, given that CK666 treatment slows spreading of coelomocytes (Figure 6), and also extend them by our demonstration of the unusual actin structural organization present in CK666-treated spreading cells (Figures 6 and 7). This actin organization is characterized by arcs similar in structure and dynamics to those present in cells treated while attached and an overall lack of the dendritic networks present in the LPs of spreading control cells (Figures 6 and 7). The CK666-treated cells do slowly spread over time, and the actin arcs create unusual patterns such as the concentric circle arrays present at the tips of substrate-associated filopodia (Figures 6 and 7).

In summary, in the present study, we demonstrate that Arp2/3 complex inhibition leads to the formation of actin arcs in coelomocytes and other cell types with broad lamellipodial regions, that these arcs are involved in cells spreading in the absence of Arp2/3 complex function, and that arc generation is arrested by formin inhibition. Our hypothetical model explaining the generation of arcs in CK666 treated cells involves the following steps: 1) CK666-induced loss of Arp2/3 complex function leads to a rapid and significant decrease in the number of sites for actin filament polymerization in the LP, given the loss of actin branch points on preexisting mother filaments; 2) actin monomers now preferentially add onto the membrane-associated barbed ends of the much fewer preexisting elongate filaments that are nucleated by formin, and this can take place in an arc and/or filopodial morphology; and 3) rapid polymerization of the actin arcs combined with a lower level of "pushing" force due to the loss of the dendritic array causes them to accumulate along the cytoplasmic face of the membrane, where their delamination and centripetal movement are driven by myosin II–based pulling from the interior of the cell. We are pursuing additional experiments to test this conceptual model.

MATERIALS AND METHODS

Animals, cell preparation, antibodies, and reagents

Sea urchins of the species *Strongylocentrotus droebachiensis* were either collected from the near-shore waters surrounding the Mount Desert Island Biological Laboratory (Salsbury Cove, ME) or obtained from the MBL Marine Resources Center (Woods Hole, MA) and kept in either running sea water or closed artificial sea water systems at 4–15°C. Coelomocytes were isolated and maintained as described in Henson *et al.* (1992) with the coelomocyte culture medium (CCM) consisting of 0.5 M NaCl, 5 mM $MgCl_2$, 1 mM ethylene glycol tetraacetic acid (EGTA), and 20 mM 4-(2-hydroxyethyl)-1-piperazineethanesulfonic acid, pH 7.2. Typically the cells were used within 24–36 h of isolation. Fish epidermal keratocytes were obtained from the scales of goldfish (*Carrasius auratus*) following the methods of Svitkina *et al.* (1997) and cultured at room temperature in DMEM plus 20% fetal bovine serum. *Drosophila* S2 cells were purchased from the American Type Culture Collection (Manassas, VA) and cultured in Schnieder's medium plus 10% fetal bovine serum at room temperature using the methods of Rogers and Rogers (2008). A rabbit polyclonal antibody against sea urchin egg myosin II heavy chain was generated from protein precipitated from sea urchin egg extracts and electrophoretically purified (Henson *et al.*, 1999). A monoclonal anti-actin antibody (clone C4) was obtained from MP Biomedicals (Santa Ana, CA), fluorescent phalloidin was purchased from Molecular Probes (Eugene, OR), TEM supplies and reagents were obtained from Electron Microscopy Sciences (Hatfield, PA), CK666, CK689, CK869, and SMIFH2 were all obtained from Calbiochem (San Diego, CA), and the majority of other reagents and antibodies were purchased from Sigma-Aldrich (St. Louis, MO).

Pharmacological treatments

For pharmacological treatments, cells being processed for fluorescence staining or electron microscopy were treated in 35-mm Petri dishes, and cells prepared for live-cell imaging were treated in simple perfusion chambers. These chambers were created by placing the coverslip containing cells on top of shims made of cut coverslips attached to a slide via petroleum jelly. Alternatively, coverslips were attached to shims made of double-stick adhesive tape. Solutions containing a drug were perfused through the chamber using the capillary action of a piece of filter paper. CK666 and CK869, the two active Arp2/3 complex inhibitors, and the inactive homologue, CK689, were made up as 50 mM stock solutions in DMSO and typically used at 100 μM (after extensive vortexing in CCM to avoid precipitation). Cytochalasin D was made up as 1 mM stock in DMSO and used at a concentration of 500 nM to 1 μM. The formin inhibitor SMIFH2 was made up as 50 mM stock solutions in DMSO and used at a concentration of 2.5–5 μM (after extensive vortexing in CCM to avoid precipitation). DMSO-alone control treatments were performed as part of every experiment involving drug treatment.

Live-cell imaging

Coelomocytes were settled onto alcohol-washed glass coverslips that were mounted on perfusion chambers and were viewed on a Nikon (Tokyo, Japan) 80i microscope using either a 40×/0.75 numerical aperture (NA) phase contrast plan objective lens or a 60×/1.4 NA phase contrast planapochromatic objective lens. Digitally enhanced phase contrast images were obtained with a Hitachi (Tokyo, Japan) charge-coupled device (CCD) camera coupled to a Hamamatsu (Hamamatsu City, Japan) Argus-10 real-time digital image processor. Frame-averaged, background-subtracted, and contrast-enhanced images were imported into ImageJ (National Institutes of Health, Bethesda, MD), where additional digital contrast enhancement and frame averaging was performed.

For axis-independent polarization microscopy and differential interference contrast (DIC) imaging, cells in perfusion chambers were viewed on an LC-PolScope (Cambridge Research and Instrumentation, Hopkinton, MA) using a strain-free 60×/1.4 NA DIC planapochromatic objective lens mounted on a Nikon Microphot SA microscope, and images were captured using a Q-Imaging (Surrey, Canada) Retiga camera and processed using Micromanager-based LC PolScope-specific software.

Fluorescence localization

For fluorescence localization of filamentous actin with phalloidin, coelomocytes were fixed with 0.25% glutaraldehyde plus 0.1%

Triton X-100 in buffer A (75 mM KCl, 2 mM $MgCl_2$, 320 mM sucrose, 20 mM EGTA, 20 mM 1,4-piperazinediethanesulfonic acid, pH 7.0) for 5 min, rinsed in phosphate-buffered saline (PBS), and then stained with Alexa Fluor 488– or 568–conjugated phalloidin. For immunofluorescence staining of Arp3 and actin, coelomocytes were prefixed in 0.000025% glutaraldehyde in CCM for 3 min (the appropriate drug treatment was added to this pre-fix to prevent recovery), fixed in 1% formaldehyde and 0.5% Triton X-100 in buffer A for 5 min, and then postfixed in 100% methanol at –20°C for 5 min. After a rinse with PBS, cells were blocked with PBS plus 1% bovine serum albumin and 2% goat serum and stained with primary antibodies, followed by the appropriate fluorescently labeled secondary antibodies. Cells were mounted in Prolong antiphotobleach containing 4′, 6-diamidino-2-phenylindole (Molecular Probes), and epifluorescence microscopy was performed on a Nikon E600 or 80i microscope using a 60×/1.4 NA planapochromatic phase contrast objective lens; digital images were captured using a Photometrics (Tucson, AZ) CoolSnap Cf cooled CCD camera. Superresolution 3D SIM was performed on a Nikon N-SIM instrument using a 100×/1.49 NA apochromatic total internal reflection fluorescence objective lens. Pixel intensity measurements for images of Arp3-stained coelomocytes were performed using ImageJ. For fixation and phalloidin staining of fish keratocytes and *Drosophila* S2 cells, we used the methods of Svitkina *et al*. (2007) and Rogers and Rogers (2008), respectively.

Transmission electron microscopy

TEM imaging of critical point-dried and rotary-shadowed replicas of coelomocyte cytoskeletons followed methods described in Henson *et al*. (1999) and Svitkina (2007). Briefly, coelomocytes settled onto glass coverslips were prefixed in 0.001% glutaraldehyde in CCM (plus appropriate drug treatments) and then extracted in 0.5% Triton X-100 in buffer A. After extraction, the cells were fixed in 2.5% glutaraldehyde in the same buffer and then treated with aqueous tannic acid, followed by aqueous uranyl acetate. Then the cells were dehydrated in a graded ethanol series, critical point dried, and rotary shadowed with platinum and carbon. Metal replicas were separated from glass coverslips using hydrofluoric acid, mounted on Formvar-coated and carbon- stabilized grids, and observed and digitally photographed on a JEOL (Tokyo, Japan) JEM-200CX TEM operating at 100 kV.

ACKNOWLEDGMENTS

We extend grateful thanks to Tanya Svitkina and Maria Shutova (University of Pennsylvania, Philadelphia, PA) for their expert assistance with the generation of platinum replicas of coelomocyte cytoskeletons, to the members of the Dickinson College Spring 2013 Biology 560 research course (Brandon Goldson, Caroline Jordan, Jake Kleiner, Christine Neville, Rebecca Patterson, and Eileen Shen) for conducting helpful preliminary experiments, to Callen Wallace and Simon Watkins (University of Pittsburgh, Pittsburgh, PA) for assistance with superresolution 3D SIM light microscopy, to Amitabh Verma and Shalin Mehta (Marine Biological Laboratory) for software engineering help with LC-PolScope acquisition, and to Louie Kerr (Marine Biological Laboratory) for excellent assistance with TEM imaging. This research was supported by National Science Foundation STEP grant 0856704 to Dickinson College, student/faculty summer research grants from the Dickinson College Research and Development Committee, Laura and Arthur Colwin Summer Research Fellowships from the Marine Biological Laboratory to J.H.H. and C.B.S., National Institutes of Health Grant EB002583 to R.O., and National Science Foundation collaborative research grants to J.H.H. (MCB-1412688) and C.B.S. (MCB-1412734).

REFERENCES

Bear JE, Gertler FB (2009). Ena/VASP: towards resolving a pointed controversy at the barbed end. J Cell Sci 122, 1947–1953.

Burnette DT, Manley S, Sengupta P, Sougrat R, Davidson MW, Kachar B, Lippincott-Schwartz J (2011). A role for actin arcs in the leading-edge advance of migrating cells. Nat Cell Biol 13, 371–381.

Chhabra ES, Higgs HN (2007). The many faces of actin: matching assembly factors with cellular structures. Nat Cell Biol 9, 1110–1121.

Edds K (1979). Isolation and characterization of two forms of a cytoskeleton. J Cell Biol 83, 109–115.

Forscher P, Smith SJ (1988). Actions of cytochalasins and colcemid on the organization of actin filaments and microtubules in a neuronal growth cone. J Cell Biol 107, 1505–1516.

Goley ED, Welch MD (2006). The ARP2/3 complex: an actin nucleator comes of age. Nat Rev Mol Cell Biol 7, 713–726.

Gupton SL, Eisenman K, Alberts A, Waterman-Storer CM (2007). mDia2 regulates actin and focal adhesion dynamics and organization in the lamella for efficient cell migration. J Cell Sci 120, 3475–3487.

Heath JP (1983). Behavior and structure of the leading lamella in moving fibroblasts. I. Occurrence and centripetal movement of arc-shaped microfilament bundles beneath the dorsal cell surface. J Cell Sci 60, 331–354.

Henson JH, Cheung D, Fried CA, Shuster CB, McClellan MK, Voss MK, Sheridan JT, Oldenbourg R (2009). Structure and dynamics of an Arp2/3 complex-independent component of the lamellipodial actin network. Cell Motil Cytoskel 66, 679–692.

Henson JH, Kolnik S, Fried C, Nazarian R, McGreevy J, Schulberg KL, Detweiler M, Trabosh VA (2003). Actin-based centripetal flow: phosphatase inhibition by Calyculin A alters flow pattern, actin organization and actomyosin distribution. Cell Motil Cytoskel 56, 252–266.

Henson JH, Nazarian R, Schulberg KL, Trabosh VA, Kolnik SE, Burns AR, McPartland KJ (2002). Wound healing in the lamellipodia of single cells: mediation by actin polymerization in the absence of an actomyosin purse string. Mol Biol Cell 13, 1015–1029.

Henson JH, Nesbitt D, Wright BD, Scholey JS (1992). Immuolocalization of kinesin in sea urchin coelomocytes: associations of kinesin with intracellular organelles. J Cell Sci 103, 309–320.

Henson JH, Schatten G (1983). Calcium regulation of the actin-mediated cytoskeletal transformation of the sea urchin coelomocyte. Cell Motil 3, 525–534.

Henson JH, Svitkina T, Burns AR, Hughes HE, McPartland KJ, Nazarian R, Borisy GG (1999). Two components of actin-based retrograde flow in sea urchin coelomocytes. Mol Biol Cell 10, 4075–4090.

Hotulainen P, Lappalainen P (2006). Stress fibers are generated by two distinct actin assembly mechanisms in motile cells. J Cell Biol 173, 383–394.

Hyatt HA, Shure MS, Begg DA (1984). Induction of shape transformation in sea urchin coelomocytes by the calcium ionphore A23187. Cell Motil 4, 57–71.

Koestler SA, Auinger S, Vinzenz M, Rottner K, Small JV (2008). Differentially oriented populations of actin filaments generated in lamellipodia collaborate in pushing and pausing at the cell front. Nat Cell Biol 10, 306–313.

Koestler SA, Steffen A, Nemethova M, Winterhoff M, Luo N, Holleboom JM, Krupp J, Jacob S, Vinzenz M, Schur F, *et al*. (2013). Arp2/3 complex is essential for actin network treadmilling as well as for targeting of capping protein and cofilin. Mol Biol Cell 24, 2861–2875.

Korobova F, Svitkina T (2008). Arp2/3 complex is important for filopodia formation, growth cone motility, and neuritogenesis in neuronal cells. Mol Biol Cell 19, 1561–1574.

Le Clainche C, Carlier M-F (2008). Regulation of actin assembly with protrusion and adhesion in cell migration. Physiol Rev 88, 489–513.

Lieber AD, Yehudai-Resheff S, Barnhart EL, Theriot JA, Keren K (2013). Membrane tension in rapidly moving cells is determined by cytoskeletal forces. Curr Biol 23, 1409–1417.

Lin CH, Espreafico EM, Mooseker MS, Forscher P (1996). Myosin drives retrograde F-actin flow in neuronal growth cones. Neuron 16, 769–782.

Machesky LM, Insall RH (1998). Scar1 and the related Wiskott-Aldrich syndrome protein, WASP, regulate the actin cytoskeleton through the Arp2/3 complex. Curr Biol 8, 1347–1356.

Nicholson-Dykstra SM, Higgs HN (2008). Arp2 depletion inhibits sheet-like protrusions but not linear protrusions of fibroblasts and lymphocytes. Cell Motil Cytoskel 65, 904–922.

Nolen BJ, Tomasevic N, Russell A, Pierce DW, Jia Z, McCormick CD, Hartman J, Sakowicz R, Pollard TD (2009). Characterization of two classes of small molecule inhibitors of Arp2/3 complex. Nature 460, 1031–1034.

Otto JJ, Kane RE, Bryan J (1979). Formation of filopodia in coelomocytes: localization of fascin, a 58,000 dalton actin cross-linking protein. Cell 17, 285–293.
Pollard TD (2007). Regulation of actin filament assembly by Arp2/3 complex and formins. Annu Rev Biophys Biomol Struct 36, 451–477.
Pollard TD, Borisy GG (2003). Cellular motility driven by assembly and disassembly of actin filaments. Cell 112, 453–465.
Ridley AJ (2011). Life at the leading edge. Cell 145, 1012–1022.
Rizvi SA, Neidt EM, Cui J, Feiger Z, Skau CT, Gardel ML, Kozmin SA, Kovar DR (2009). Identification and characterization of a small molecule inhibitor of formin-mediated actin assembly. Chem Biol 16, 1158–1168.
Rogers SL, Rogers GC (2008). Culture of *Drosophila* S2 cells and their use for RNAi-mediated loss-of-function studies and immunofluorescence microscopy. Nat Procot 3, 606–611.
Rogers SL, Wiedemann U, Stuurman N, Vale RD (2003). Molecular requirements for actin-based lamella formation in *Drosophila* S2 cells. J Cell Biol 162, 1079–1088.
Small JV, Resch GP (2005). The comings and goings of actin: coupling protrusion and retraction in cell motility. Curr Opin Cell Biol 17, 517–523.
Steffen A, Faix J, Resch GP, Linkner J, Wehland J, Small JV, Rottner K, Stradal TE (2006). Filopodia formation in the absence of functional WAVE- and Arp2/3-complexes. Mol Biol Cell 17, 2581–2591.
Strasser GA, Rahim NA, VanderWaal KE, Gertler FB, Lanier LM (2004). Arp2/3 is a negative regulator of growth cone translocation. Neuron 43, 81–94.
Suraneni P, Rubinstein B, Unruh JR, Durnin M, Hanein D, Li R (2012). The Arp2/3 complex is required for lamellipodia extension and directional fibroblast cell migration. J Cell Biol 197, 239–251.
Svitkina T (2007). Electron microscopic analysis of the leading edge in migrating cells. Methods Cell Biol 79, 295–319.
Svitkina TM (2013). Ultrastructure of protrusive actin filament arrays. Curr Opin Cell Biol 25, 1–8.
Svitkina TM, Verkhovsky AB, McQuade KM, Borisy GG (1997). Analysis of the actin-myosin II system in fish epidermal keratocytes: mechanism of cell body translocation. J Cell Biol 139, 397–415.
Vinzenz M, Nemethova M, Schur F, Mueller J, Narita A, Urban E, Winkler C, Schmeiser C, Koestler SA, Rottner K, *et al*. (2012). Actin branching in the initiation and maintenance of lamellipodia. J Cell Sci 125, 2775–2785.
Wu C, Asokan SB, Berginski ME, Haynes EM, Sharpless NE, Griffith JD, Gomez SM, Bear JE (2012). Arp2/3 is critical for lamellipodia and response to extracellular matrix cues but is dispensable for chemotaxis. Cell 148, 973–987.
Yang C, Czech L, Gerboth S, Shin-ichiro K, Scita G, Svitkina T (2007). Novel roles of formin mDia2 in lamellipodia and filopodia formation in motile cells. PLoS Biol 5, 2624–2645.
Yang Q, Zhang XF, Pollard TD, Forscher P (2012). Arp2/3 complex-dependent actin networks constrain myosin II function in driving retrograde actin flow. J Cell Biol 197, 939–956.
Yarrow JC, Lechler T, Li R, Mitchison TJ (2003). Rapid de-localization of actin leading edge components with BDM treatment. BMC Cell Biol 4, 5.